Available online at www.sciencedirect.com
ScienceDirect
Journal of Power Sources 159 (2006) 282–286
JOURNAL OF POWER SOURCES
www.elsevier.com/locate/jpowsour

Short communication

A study on $LiFePO_4$ and its doped derivatives as cathode materials for lithium-ion batteries

G.X. Wang [a,*], S. Needham [a], J. Yao [a], J.Z. Wang [a], R.S. Liu [b], H.K. Liu [a]

[a] *Institute for Superconducting & Electronic Materials, University of Wollongong, NSW 2522, Australia*
[b] *Department of Chemistry, National Taiwan University, Taipei, Taiwan*

Available online 5 June 2006

Abstract

$LiFePO_4$, doped $LiM_xFe_{1-x}PO_4$, and $Li_{1-x}M_xFePO_4$ compounds have been prepared via a sol–gel synthesis method. The physical properties of the as-prepared lithium iron phosphates were characterised by X-ray diffraction, X-ray absorption near-edge spectroscopy (XANES), and magnetic susceptibility. The electrochemical properties lithium iron phosphates were tested by a variety of electrochemical techniques. Lithium iron phosphate electrodes demonstrated a stable discharge capacity of 160–165 mAh g^{-1}, almost approaching the theoretical capacity. The good electronic conductivity and nanocrystalline could contribute to the unique performance of lithium iron phosphate electrodes. Lithium iron phosphates have a significant potential to be used as a new cathode materials in Li-ion batteries.

Keywords: Lithium iron phosphates; Lithium-ion batteries; X-ray absorption near-edge spectroscopy; Magnetic susceptibility

1. Introduction

Lithium-ion batteries are state-of-the-art power sources for modern portable electronic devices. In the lithium-ion battery, lithium ions shuttle between cathode and anode hosts via intercalation and de-intercalation. The cathode host provides lithium ion sources for battery operation. Currently, lithium-ion batteries employ $LiCoO_2$ as cathode material and carbon as anode material, which limits applications to small-scale batteries due to high cost and toxicity of Co [1,2]. Recently, lithium polyanion compounds with the general formula $Li_xM_y(XO_4)_z$ (M: transition metal; X: P, S, As, Mo, or W) have been investigated as novel cathode materials for lithium-ion batteries. Among them, lithium iron phosphate attracted a particular interest. $LiFePO_4$ has an orthorhombic olivine structure, in which Li, Fe, and P atoms occupy octahedral 4a, octahedral 4c, and tetrahedral 4c sites. The strong P–O covalency stabilizes the anti-bonding Fe^{3+}/Fe^{2+} state through the Fe–O–X inductive effect to generate high operating potential (3.4–3.5 V versus Li/Li^+). $LiFePO_4$ cathode materials have a high theoretical capacity of 170 mAh g^{-1} and are environmentally benign, inexpensive and naturally abundant. However, $LiFePO_4$ has a poor electronic conductivity, significantly influencing its rate capacity and applications. Many efforts have been made to improve the performance of $LiFePO_4$ cathode materials, including addition of conductive Cu/Ag powders and carbon black powders, supervalence cation doping, carbon coating, and synthesis of nanocrystalline grains [3–8]. In this paper, we describe the synthesis, physical characteristics and electrochemical properties of $LiFePO_4$ and its doped derivatives.

2. Experimental

$LiFePO_4$, $LiM_xFe_{1-x}PO_4$, and $Li_{1-x}M_xFePO_4$ compounds were prepared via a sol–gel preparation route. $Li(OH)\cdot H_2O$ (99.9%, Aldrich), $FeC_2O_4\cdot 2H_2O$ (99%, Aldrich), $NH_4\cdot H_2PO_4$ (97%, Aldrich), $Mg(C_2H_3O_2)_2$ (99%, Aldrich), $Ti(OCH_3)_4$ (99%, Aldrich), and $Zr(OC_2H_5)_4$ (99%, Aldrich) were used as reactants. The stoichiometric reactants were dissolved in deionised water, in which polyacrylic acid and citric acid were added as complexing agents for the formation of the gel. The solutions were heated and maintained at 85 °C under vigorous stirring until a viscous gel was formed. The as-formed gel was heated to 500 °C to decompose the organics under flowing argon gas. The decomposed precursors were further sintered at 700 °C, under a flowing gas mixture (10% H_2 in Ar). A slightly reducing atmosphere was employed during the sintering process in

* Corresponding author. Fax: +61 2 4221 5731.
E-mail address: gwang@uow.edu.au (G.X. Wang).

0378-7753/$ – see front matter © 2006 Elsevier B.V. All rights reserved.
doi:10.1016/j.jpowsour.2006.04.046

order to prevent the oxidation of Fe^{2+} cations. X-ray diffraction was performed on the prepared lithium iron phosphates to determine the phase purity using Cu Kα radiation (MO3xHF22, MacScience, Japan). X-ray absorption experiments were carried out at the National Synchrotron Radiation Research Centre (Taiwan). The electron storage ring was operated at an energy of 1.5 GeV with a beam current of 100–200 mA at the Wiggler beam line BL 17 C. A Si(1 1 1) double-crystal monochromator was used for energy selection with a resolution ($\Delta E/E$) of about 2×10^{-4}. The XANES spectra at the Fe–K-edge were recorded at room temperature in transmission mode using gas-filled ionization chambers to measure the intensities of the incident (I_0), transmitted (I_t), and reference (I_{ref}) signals. The morphology of lithium iron phosphate powders was studied using a scanning electron microscope (JEOL JEM-3000). The magnetic properties of lithium iron phosphates were studied using a Quantum Design MPMS XL SQUID magnetometer. The dc susceptibility was measured in a magnetic field of 5000 Oe from 5 to 300 K. Electrochemical characterisation was performed by assembling CR2032 coin cells for galvanostatic charge/discharge. The electrodes were made by dispersing 80 wt.% active material, 10 wt.% carbon black and 10 wt.% polyvinylidene fluoride (PVDF) in *n*-methyl pyrrolidone (NMP) to form a slurry. The slurry was then coated onto an Al foil. The coated electrodes were dried in a vacuum oven and then pressed at 1200 kg cm^{-2}. The coin cells were assembled in an argon-filled Glove-box (Mbraun, Unilab, Germany) with lithium foil as the counter electrode. The electrolyte was 1 M $LiPF_6$ in a 1:1 mixture of ethylene carbonate (EC) and dimethyl carbonate (DMC).

3. Results and discussion

X-ray diffraction patterns of $LiFePO_4$, $LiM_xFe_{1-x}PO_4$, and $Li_{1-x}M_xFePO_4$ compounds are shown in Fig. 1. All diffraction lines are indexed to an orthorhombic crystal structure (space group: *pnma*). Previously, there was report that some detectable impurities such as Li_3PO_4 has been identified in doped $LiFePO_4$ prepared by solid-state reaction. In contrast, we did not detect any impurities, indicating that our wet chemical preparation route can produce purer compounds than the solid-state reaction process. In the triphylite $LiFePO_4$ crystal structure, Fe^{2+} ions are located at FeO_6 octahedron (4c), and Li^+ ions occupy

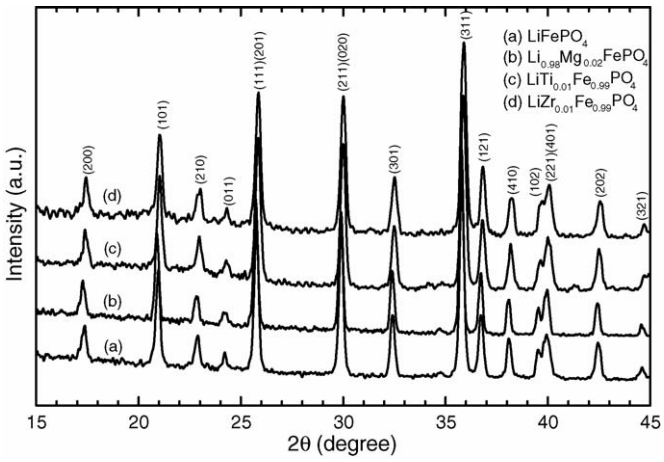

Fig. 1. X-ray diffraction patterns of lithium iron phosphate compounds.

octahedral (4a) sites. For Ti^{4+} and Zr^{4+} doping, we intended to substitute at Fe^{2+} sites, whereas for Mg^{2+} doping, we intended to substitute at Li^+ sites. This is designed to induce different level of vacancies in the crystal structure. The morphologies of lithium iron phosphates were observed by scanning electron microscope. Fig. 2 shows SEM images of lithium iron phosphates. Well-crystallized powders were obtained after sintering at 700 °C. The average crystal size of lithium iron phosphates is in the range of 1–3 μm. Thermogravimetry analysis was performed on the as-prepared lithium iron phosphate compounds. In general, the samples contain 3 wt.% carbon, which is introduced by the decomposition of organic precursors.

The temperature dependencies of the molar magnetic susceptibilities of $LiFePO_4$ sample are shown in Fig. 3. The reciprocal susceptibility and the effective magnetic moment are shown in the inset. The magnetic susceptibility of $LiFePO_4$ shows a maximum at 50 ± 2 °K (Néel temperature, θ_N), indicating a paramagnetic–antiferromagnetic phase transition. A typical Curie–Weiss law behaviour is followed above the Néel temperature. The measured effective magnetic moment μ value is 4.9 μ_B at room temperature. There are six electrons in 3d orbitals for the Fe^{2+} ion. Due to the influence of the octahedral crystal field in $LiFePO_4$ structure, the five 3d orbitals of the Fe^{2+} ion split into three t_{2g} and two e_g configurations. Among them, four electrons are on the three t_{2g} orbitals (d_{xy},

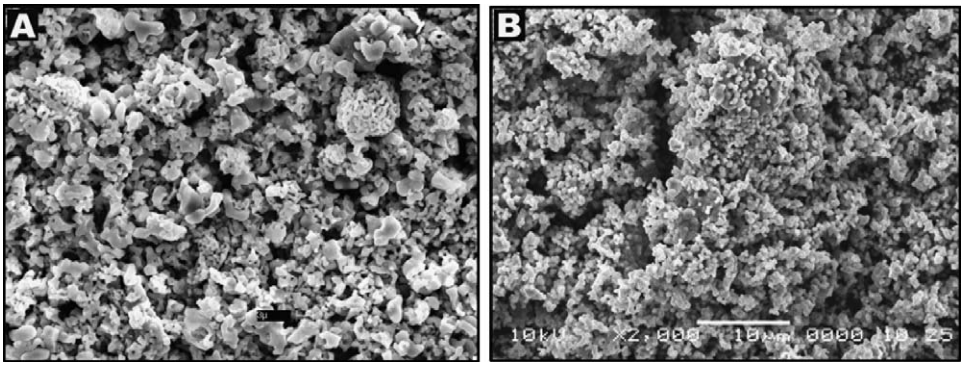

Fig. 2. SEM images of: (A) $LiFePO_4$ and (B) $Li_{0.98}Mg_{0.02}FePO_4$.

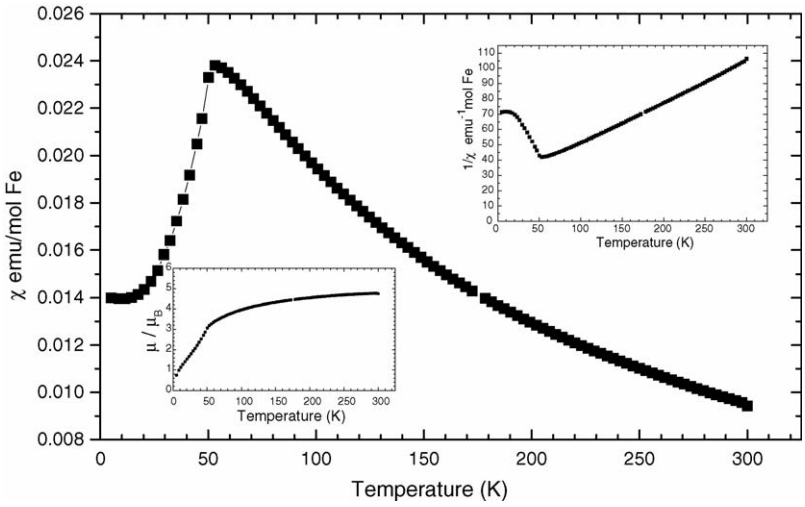

Fig. 3. Temperature dependencies of molar magnetic susceptibilities of $LiFePO_4$ sample. The insets are reciprocal magnetic susceptibilities and effective magnetic moment.

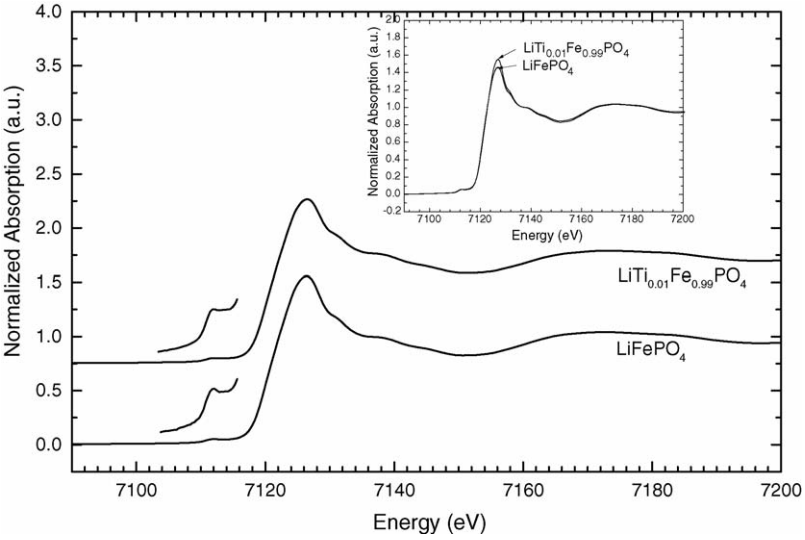

Fig. 4. Fe–K-edge XANES spectra of $LiFePO_4$ and doped $LiTi_{0.01}Fe_{0.99}PO_4$ samples.

d_{xz}, and d_{yz}), in which three electrons spin up and the fourth electron spins down. The magnetic moments for the paired two electrons in one of the t_{2g} orbitals cancel each other. Therefore, there are a net two spin-up electrons in t_{2g} orbitals. Two electrons occupy two e_g orbitals ($d_{x^2-y^2}$ and d_{z^2}), in which one electron is in each orbital with spin-up configuration. The Fe^{2+} ion presents a net four spin-up electrons (high spin), with an expected magnetic moment of 4 μ_B on the basis of the spin-only value. However, the measured magnetic moment is 4.9 μ_B, which is higher than the theoretical value. Since the angular momentum for the Fe^{2+} ion is not equal to 0, the Fe^{2+} ion could have a strong spin–orbit coupling, inducing anisotropy and a non-quenched angular momentum. An orbital momentum could contribute to the measured magnetic moment. Following the super and super–super exchange rule, the interactions between Fe–O–Fe induce antiferromagnetism, as exhibited by the magnetic measurement. However, in the orthorhombic phase, there is no Fe–O–Fe bonding, only Fe–O–P–O–Fe bonding. So, the

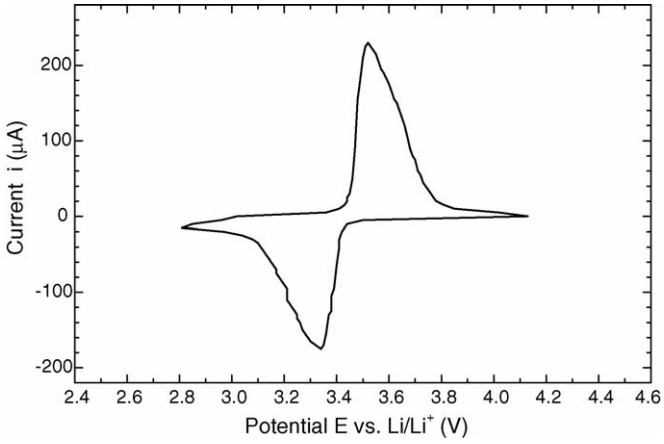

Fig. 5. Cyclic voltammogram of $LiFePO_4$ electrode.

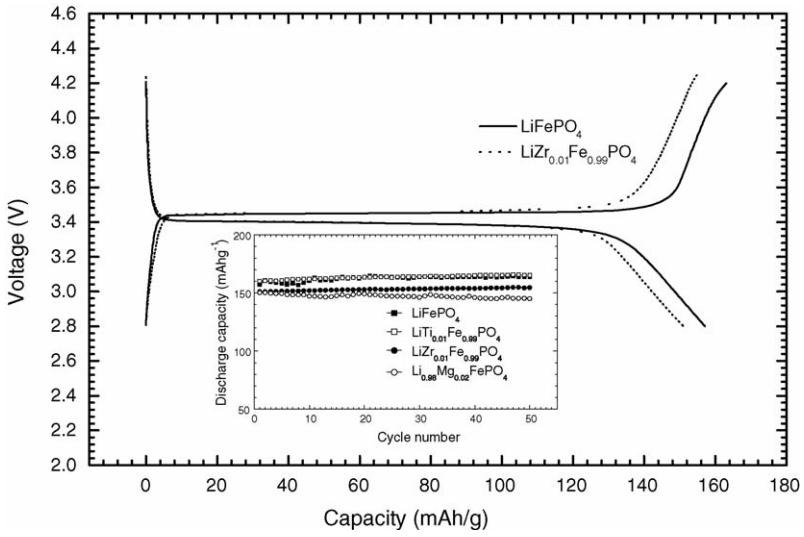

Fig. 6. The charge/discharge profiles in the first cycle for $LiFePO_4$ and doped $LiZr_{0.01}Fe_{0.99}PO_4$ electrodes. The inset shows the discharge capacities vs. cycle number for all lithium iron phosphate cathodes.

magnetic interaction in $LiFePO_4$ could be long-range through Fe–O–P–O–Fe triple exchange [9,10].

Fe–K-edge XANES of the pristine $LiFePO_4$ and $LiTi_{0.01}Fe_{0.99}PO_4$ samples are shown in Fig. 4. In order to identify the features of the pre-edge, the pre-edge region of the spectra was magnified by 10 times in Fig. 4. The energy positions of the maxima of the pre-edge peak are most sensitive to the Fe oxidation state, while the pre-edge peak's intensity is most sensitive to site centrosymmetry, with the most centrosymmetric Fe coordinations having the lowest intensity. Therefore, it will be at the lowest intensity for octahedral symmetry (O_h) and reach the maximum in the case of tetrahedral coordination (T_d). The pre-edge peak position observed is 7111.9 eV for both $LiFePO_4$ and $LiTi_{0.01}Fe_{0.99}PO_4$. It is in the same energy range observed for Fe^{2+} previously, which proves that the valence of Fe in $LiFePO_4$ and $LiTi_{0.01}Fe_{0.99}PO_4$ is +2. There is no variation of pre-edge energy position and pre-edge intensity due to Ti doping, which confirms that the trace amount of dopant Ti^{4+} ions does not disturb the oxidation state of Fe or the structural coordination in $LiFePO_4$ crystals. The Fe pre-edge peak represents $1s \rightarrow 3d$ quadrupolar electronic transitions to the t_{2g} levels. It is a dipole forbidden process. However, it becomes partially allowed due to the mixing of d-states of Fe with the p-states of the surrounding oxygen atoms. The pre-edge energy for Fe^{3+} in $FePO_4$ is located at 7114.2 eV [11], which is 2.3 eV higher than that of Fe^{2+} in $LiFePO_4$. This is ascribed to the fact that the electrons in Fe^{3+} ions are strongly bound to the nucleus, inducing the shift of $1s \rightarrow 3d$ transitions to a higher energy level. The inset in Fig. 4 shows a comparison of the Fe–K-edge XANES spectra of undoped $LiFePO_4$ and doped $LiTi_{0.01}Fe_{0.99}PO_4$. The Fe–K-edge XANES spectra consist of two main parts—the pre-edge and the main edge regions. The pre-edge is located to the lower energy side of the sharply rising absorption edge, corresponding to a $1s \rightarrow 3d$-type electronic transition. The main edge region extends a few tens of electron volts higher above the pre-edge, mainly corresponding to multiple-scattering resonances of photoelectrons ejected with low kinetic energy. It is also called the white line. The doped $LiTi_{0.01}Fe_{0.99}PO_4$ exhibits an increased white line (~7125 eV) intensity over that of undoped $LiFePO_4$. The increasing of the white line intensity reflects the increased number of unoccupied d-states for Fe ions in the crystal structure [12]. The 3d and 4s orbits are all empty in Ti^{4+} ions. There are four valence electrons in 3d orbit in Fe^{2+} ions. Therefore, when Ti^{4+} is substituted for Fe^{2+}, Ti^{4+} ions would be able to attract 3d electrons from Fe^{2+}, creating positive holes in the 3d-states in Fe ions. This effect induces an increased p-type semiconductivity. Previously, Chiang and co-workers found that supervalent ion doping of $LiFePO_4$ compounds results in extrinsic p-type semiconductors [7]. Our Fe–K-edge XANES measurement has confirmed this finding.

Cyclic voltammetry measurements were performed on lithium iron phosphate electrodes to characterise the electrochemical reactions in Li-ion calls. Fig. 5 shows the typical cyclic voltammograms (CV) of $LiFePO_4$ electrodes. The reduction and oxidation peak positions are located at 3.34 and 3.52 V, respectively, versus Li/Li^+. The specific capacities and cyclabilities of lithium iron phosphate electrodes were tested by constant current charge/discharge cycling at a *C*/8 rate. Fig. 6 shows the voltage profiles of $LiFePO_4$ and $LiZr_{0.01}Fe_{0.99}PO_4$ electrodes in the first cycle. The voltage profiles exhibit very flat charge and discharge plateaus, matching the oxidation and reduction peaks in the CV curves. The cyclabilities of all lithium iron phosphates are shown in the inset in Fig. 6. Lithium iron phosphates demonstrated a stable specific capacity in the range of 150–160 mAh g^{-1}, which is higher than $LiCoO_2$ cathode materials. Therefore, lithium iron phosphate cathode materials show promising as a new cathode material for lithium-ion batteries.

4. Conclusions

A series of lithium iron phosphate cathode materials have been prepared via a sol–gel synthesis route. The supervalent doping results in an increased p-type semiconductivity for lithium

iron phosphates, which has been confirmed by X-ray absorption near edge spectroscopy measurement. Lithium iron phosphates demonstrated typical antiferromagnetic behaviour with $\theta_N = 50 \pm 2$ K. Lithium iron phosphates are electrochemically active with a specific capacity in the range of 150–160 mAh g^{-1}.

Acknowledgement

This work was financially supported by the Australian Research Council through the ARC Centre for Nanostructured Electromaterials and ARC Linkage Project (LP0453766).

References

[1] J.-M. Tarascon, M. Armand, Nature 414 (2001) 359–367.
[2] M.S. Whittingham, Chem. Rev. 104 (2004) 4271–4301.
[3] A.K. Padhi, K.S. Nanjandaswamy, J.B. Goodenough, J. Electrochem. Soc. 144 (1997) 1188.
[4] A.K. Padhi, K.S. Nanjandaswamy, C. Masquelier, J.B. Goodenough, J. Electrochem. Soc. 144 (1997) 1609.
[5] F. Croce, A. D'Epifanio, J. Hassoun, A. Deptula, T. Olczac, B. Scrosari, Electrochem, Solid State Lett. 5 (2002) A47.
[6] S. Franger, F. Le Cras, C. Bourbon, H. Rouault, Electrochem. Solid State Lett. 5 (2002) A231.
[7] S.-Y. Chung, J. Bloking, Y.-M. Chiang, Nat. Mater. 1 (2002) 123.
[8] H. Huang, S.C. Yin, T. Kerr, N. Taylor, L.F. Nazar, Adv. Mater. 3 (2004) 147.
[9] G. Rousse, J. Rodriguez-Carvajal, S. Patoux, C. Masquelier, Chem. Mater. 15 (2003) 4082.
[10] R.P. Santoro, R.E. Newnham, Acta Cryst. 22 (1967) 344.
[11] G. Berlier, G. Spoto, P. Fisicaro, S. Bordiga, A. Zecchina, E. Giamello, C. Lamberti, Microchem. J. 71 (2002) 101.
[12] A.N. Mansour, J.W. Cook, D.E. Sayers, J. Phys. Chem. 88 (1984) 2330.